Case Studies in Thermal Engineering 28 (2021) 101436

Contents lists available at ScienceDirect

Case Studies in Thermal Engineering

journal homepage: www.elsevier.com/locate/csite

# Synthesis of graphene oxide nanofluid based micro-nano scale surfaces for high-performance nucleate boiling thermal management systems

Shoukat Alim Khan, Sami G. Al-Ghamdi *

*Division of Sustainable Development, College of Science and Engineering, Hamad Bin Khalifa University, Qatar Foundation, Doha, Qatar*

ARTICLE INFO

*Keywords:*
Nanofluid
Phase change heat transfer
Concentrated photovoltaics
Micro-nano coatings
Renewable energy

ABSTRACT

The objective of this study is to explore the exceptional thermal management ability of Graphene Oxide (GO) nanofluid and microporous surfaces (M) for nucleate pool boiling based thermal management systems. The performance of the designed system has been analyzed for thermal management of concentrated photovoltaics (CPV) system. A detailed analysis has been performed for GO nanofluid, with concentrations; 0.0001%, 0.001%, and 0.01%, and deionized (DI) water-based working fluid over the plane unmodified surface (P) and microporous (M) surfaces. GO nanofluid enhanced critical heat flux (CHF) and the heat transfer coefficient (HTC) over the plane surface. However, over M surface, GO nanofluid resulted in thick layer formation and significantly affected the NBHT performance. The highest CHF of 1850 kW/m$^2$ has been observed for GO over the plane surface, increasing 2.31 times. M surface with deionized water resulted in the highest average HTC of 64.36 kW/m$^2$.K, increasing 3.47 times. GO over the plane surface ($N_p$) based NBHT thermal management system resulted in the highest concentration ratio of 3102 and can be used for CPV system. In comparison, M surface-based thermal management system resulted in the highest efficiency.

## 1. Introduction

Globally, the urban population has already exceeded the rural population for the first time in history. This brought a remarkable transformation in economic, social and technological challenges in cities. Among these, the supply of sustainable and renewable energy is one of the critical challenges. In renewable energy-based solutions, photovoltaic technology is one of the promising technology. However, a larger installation area, due to its low efficiency is a challenge in urban infrastructure [1]. A multi-junction solar cell (MJSC) is used in photovoltaics technology where high electrical efficiency is required in less available space, such as aerospace applications. Recently, multifunction solar cells (MJSC) have achieved efficiency above 48% and is increasing continuously, with an average of 1% per year. With increasing efficiency, multifunction solar cell (MJSC) based photovoltaic technology can limit installation area requirements. However, due to their high prices, MJSC is used by concentrated photovoltaics (CPV) technique. To replace the required cell area, optical devices i.e. lenses or mirrors, are used to concentrate the light on a small cell. The high concentration of sunlight also generates extraordinary heat flux in a small cell area. Hence, an effective thermal management system is one of the core requirements of these systems [2,3].

* Corresponding author.
*E-mail address:* salghamdi@hbku.edu.qa (S.G. Al-Ghamdi).

https://doi.org/10.1016/j.csite.2021.101436
Received 18 January 2021; Received in revised form 26 August 2021; Accepted 8 September 2021
Available online 11 September 2021

Phase change heat transfer based thermal management systems are prevalent in many applications, including fusion reactor, nuclear power plants, data centers, supper computers, concentrated photovoltaic systems, advanced radar systems, spacecraft avionics and aircraft, power electronics of electric and hybrid vehicles, turbine and engine head cooling, X-ray devices and quenching of metals alloy [4–7]. The maximum ability of heat transfer and efficient heat removal is the key parameters of the thermal management system. In CPV system, both of these parameters are highly sensitive to the feasibility of CPV based system installation. The maximum ability of heat transfer is directly related to the maximum possible concentration in CPV system. The increase in concentration decreases the required cell material in CPV system, which is the most expansive part of CPV. On the other hand, the efficient removal of heat flux results in lower cell temperature. And lower cell temperature results in higher electrical efficiency and hence the resultant electrical energy output [7,8].

NBHT is a practical phase-change transfer technique. The performance enhancement of NBHT comprises several goals, including the early nucleation of nucleate boiling, lowering the wall superheat, increase in HTC and delaying CHF to higher heat flux values [9]. CHF represents the maximum limit of heat transfer in NBHT process and HTC represents the efficiency of the heat transfer in NBHT. In thermal management of CPV using NBHT, CHF is directly related to the maximum possible concentration of light i.e. concentration ratio. While high HTC value ensures the lower working temperature of the cell and hence high electrical efficiency.

The enhancement techniques for pool boiling can be classified in active and passive techniques. Working fluid or surface modification are two main techniques for performance enhancement by Passive technique.

Nanoscale structures for pool boiling are introduced with discoveries; however, as the phenomena are not fully understood, most of the studies focused on experimental work [10]. Nanoscale surface coatings and working fluid modification techniques are primarily explored for this purpose [11,12]. Das et al. [13] and You et al. [14] were first to examine nanofluid performance in pool boiling. Since then, nanomaterials with chemically stable metals (e.g. Cu, silver, gold), metal oxides (e.g. silica, alumina, titania, zirconia) and carbon-based (e.g., carbon nanotubes, graphene, carbon black, fullerene) are reported in the literature for NBHT performance enhancement. Lian and Mudawar [15] compiled a comprehensive review on modifying fluid properties by a nanofluid, polymer additives, and surfactants to enhance nucleate pool boiling.

You et al. [14] reported up to 200% enhancement in CHF for alumina nanofluid with a minimal concentration of 0.005%. Vassallo et al. [16] reported 60% enhancement in CHF with 0.5 vol% of $SiO_2$ nanofluid. Both studies reported no significant increase in HTC. Lee et al. [16] reported an increase in bubbles frequency to double for alumina and $Fe_3O_4$ nanofluid. The decrease in bubble size is coupled with an increase in the frequency of the bubble. The enhancement in performance was noticed only for low concentration of nanofluid, i.e. up to 0.01 g/l, above that the increase in concentration was not advantageous.

Graphene oxide (GO) and carbon nanotubes (CNT) are widely explored carbon-based nanoparticles in NBHT. Functionalized CNT are commonly used in these experiments to have better dispersion in water. CNT based nanofluid are reported with an increase in CHF performance. Liu et al. [17] investigated the performance of nitric acid-treated CNT for a wide range of concentrations from 0.5 to 4.0 wt% and working pressure from 7.4 to 103 kPa. The highest version is reported for 2.0 wt%. The study also compared the performance with CNT coated surface and reported better performance for nanofluid. Kamatchi et al. [18] examined the effect of concentration of GO nanofluid from 0.001 to 0.3 g/l and reported enhancement in CHF of 145–245%. Similarly, Park et al. [19] examined the effect of modification in the working fluid of GO on NBHT performance. The water-based working fluid is modified with the addition of trisodium phosphate, lithium hydroxide, and boric acid to explore different coolant performances. They reported not only the stability of GO but also further enhancement in CHF performance. The researcher reported various working fluids and carbon-based (i.e. carbon nanofibers, carbon black) nanofluid with better version of CHF, HTC and superheat value [20–23].

Nanofluid results in the deposition over the heating surface and increases the overall surface area, surface roughness and nucleation sites for bubbles. This results in an increase in bubbles density, smaller bubbles diameter and hence high bubbles frequency, which contributes to the increase in heat transfer performance in terms of CHF, HTC and lower superheat value. Even though the significant improvement in CHF reported for most of nanofluid, there are some contradictory findings for HTC. The contradictions are the result of the complex influence of surface roughness, base liquid and nanofluid.

Like working fluid modification, there is abundant evidence of an increase in heat transfer by surface modification, i.e. extended surface area, nanoparticles coatings, micro-fins and microporous surface. Wen et al. [24] analyzed the performance of patterned Cu nanowires with two-level hierarchical structures. The reported liquid rewetting and bubbles nucleation with 185% enhancement in HTC and 71% in CHF. Similarly, in another study Wen et al. [25] analyzed boiling heat transfer performance for Cu micro meshes fabricated with the etching process. The enhancement in CHF and HTC is reported to be enhanced by increasing bubbles density and liquid supply. Micro-porous surface helps separate bubbles and liquid flows and help in providing separate pathways for bubbles and working. This helps in an increase in delaying the critical heat flux. In addition, it also helps in an increase in bubbles nucleation sites and overall surface area. Suraj et al. [26] performed NBHT experiments on Cu microporous surfaces using HFE-7100 as working fluid. The study reported enhanced results in boiling incipience temperature and CHF compared to plain surface. The CHF is reported to increase by 50%–270% for different experimental conditions. Bergles and Chyu [27] analyzed pool boiling over porous Cu coating with different thicknesses. The study reported 0.38 mm as optimum thickness in terms of HTC enhancement. 250% enhancement in CHF is reported for water and 800% for R-113 as the working fluid.

Keeping in view the individual enhanced performance of both GO nanofluid and micro-porous surfaces, the objective of this study is to experimentally explore the NBHT performance of GO nanofluid over a micro-porous surface with the hypothesis of improved performance. The objective of the study also included the detailed analysis of the developed system for thermal management performance of CPV and investigated their effect on the critical installation parameters of the installation area and cost in urban infrastructure.

In the first part of the study, the synthesis of surface and working fluid their experimental analysis in NBHT is performed. The

experimental results are then coupled with the analytical model of CPV to analyze the targeted CPV performance analysis.

## 2. Design and synthesis of surfaces and CPV performance analysis

Table 1 summarized four types of surfaces experimentally tested in this study for NBHT.

**Nanofluid Preparation:** Three different concentration of GO nanofluid were prepared with a concentration of 0.0001%, 0.001% and 0.01%. GO were purchased form The Sixth Element Inc. Deionized water was used as base fluid for the dispersion of GO to prepared the nanofluid. Probe type sonicator is used in all the three cases with ON: OFF ratio of 3:1 for 4 h.

**Microporous (M) surface:** The detail synthesis technique and the experimental procedure can be found in the previous publication of the group [28]. Microporous surface of prepared by the hot powder compaction technique, using Cu microparticles with an average size of 200 μm (range: 150–249 μm). The oxide layer has been removed by the thermal reduction in an inert environment with 5% hydrogen. The microporous surface samples were placed in tube furnace at 250 $^{O}$C for 4 h.

**Hybrid (H) surface:** The use of GO nanofluid over M surface resulted in new Hybrid (H) micro-nano surfaces. In the NBHT experiment, GO resulted in the deposition over the boiling surface and form H surface. The deposition of nanoparticles during boiling was made confirmed by SEM analyses after the experiment. During these experiments, three different concentrations of 0.001%, 0.01%, and 0.1% of GO nanofluid were tested and analyzed.

## 3. Experimental procedure

The experimental process is briefly explained here, detail analysis and calculations can be found in the previous publications [8,29, 30].

### 3.1. Experimental setup

The Cu block was used as a heating element for the testing surface. Four symmetrical holes were made in Cu block where cartridge heaters were inserted. Thermal paste is used to fill the air gap between the heaters and sidewalls of holes. The Cu block and working fluid container's supported assembly is made of Teflon due to its high thermal conductivity and easy machining. Pyrex glass is used as a container for working fluid. The Cu block is further insulated with glass fibers. Thermal simulations were performed at extreme working conditions to ensure safe operation with Teflon. Two thermocouples were inserted near the top surface of the Cu block to measure the surface temperature. The top section of the Cu block was manufactured in square shape $2 \times 2$ cm$^2$. The testing sample is placed on top of the Cu block for direct interaction with working fluid. Before the start of the experiment, the testing sample is fixed on the top of the Cu block by soldering. Soldering material is applied between the model and block, and heat is applied using input electrical power until the soldered material is melted, and then the testing sample is gently pressed for more solid contact. The testing sample is firmly attached to the Cu block with a very thin and highly conductive metallic layer of soldering material upon natural cooling. A Pyrex glass is used as a container for working fluid. The system is connected with a chiller to condensate the liquid back to the experimental system after evaporation.

The input power, in the form of electrical energy, is controlled by a variable voltage transformer. An ammeter and voltmeter are connected to ensure accurate measurement. A high-speed camera is used to analyze the bubble's dynamics, Fig. 1. The input power is gradually raised, and the corresponding temperature is noted until the CHF is reached. Each temperature reading ensures that the related fluctuation is minor than ±0.2 °C for 3 min.

### 3.2. Data calculation and uncertainties

The temperature readings, T1 and $T_2$, from two thermocouples near the heating surface are used to calculate the heating surface temperature by one-dimensional temperature distribution [31]:

$$T_{b.surface} = T_1 - \left(\frac{T_2 - T_1}{\Delta x_{12}}\right)\Delta x_{1s} \quad (1)$$

where $T_{b.surface}$ the temperature of the tasting sample, ΔX represents the distance between two thermocouples ($\Delta X_{12}$) and thermocouple 1 and testing sample ($\Delta X_{1s}$).

Fourier law is applied to calculate the total heat transfer:

**Table 1**
NBHT experiments performed for the study and their experimental conditions.

| | | Representation | Experimental conditions |
|---|---|---|---|
| 1 | Plain Cu surface | P | Testing surface: Plain Cu; Working fluid: deionized water |
| 2 | Microporous surface | M | Testing surface: Cu micro-porous surface; Working fluid: deionized water |
| 3 | Nanofluid | $N_P$ | Working fluid: GO nanofluid; Testing surface P |
| 4 | Hybrid | H | Working fluid: GO nanofluid; Testing surface M |

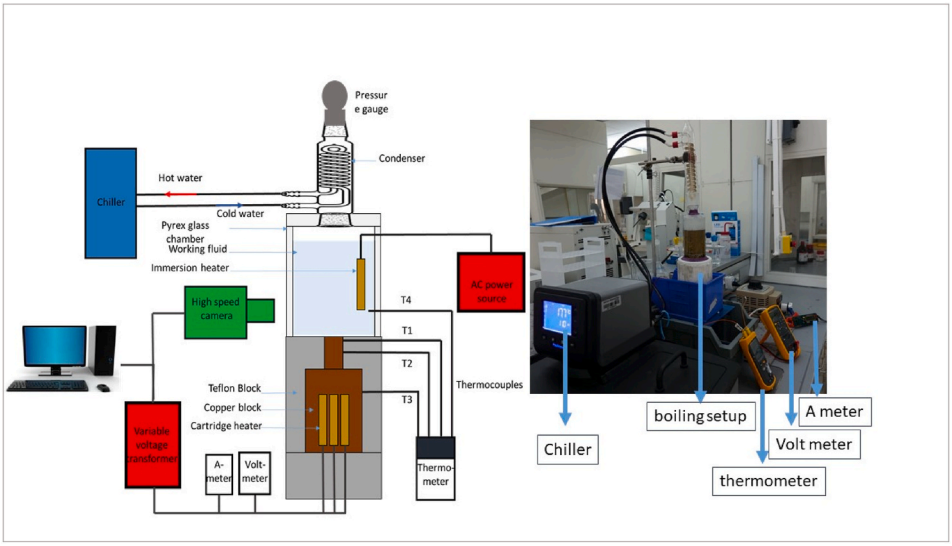


**Fig. 1.** NBHT experimental setup used to conduct the study, sketch up and an original picture.

$$P_{out} = k_{Cu}\frac{T_1 - T_{b,surface}}{\Delta x_{1s}} \tag{2}$$

where $K_{Cu}$ represents the thermal conductivity of Cu (kW/m•K). The calculation is cross-checked with the input voltage (V) and current (I) calculated by the attached voltmeter and Ammeter to the system by:

$$P_{out} = V * I \tag{3}$$

HTC is calculated by:

$$HTC = \frac{q''}{T_{b.surface} - T_{sat}} \tag{4}$$

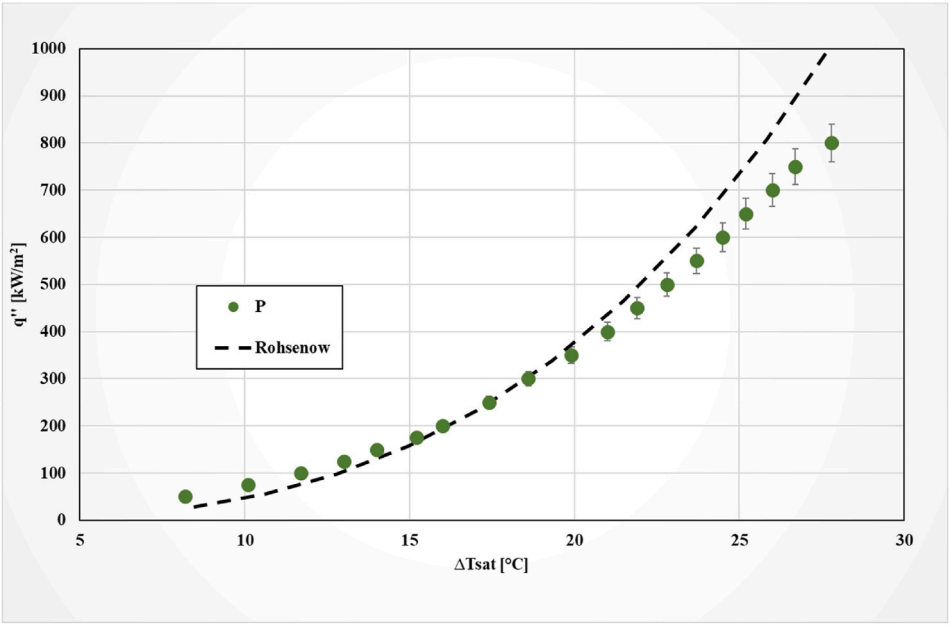


**Fig. 2.** Comparison of the experimental data with standard Rohsenow correlation to ensure the reliability of the experimental setup and calculated data.

where $T_{sat}$ is working fluid's saturation temperature and $q''$ represents heat flux calculated by:

$$q'' = \frac{P_{out}}{A} \tag{5}$$

A is the cross-section area of the testing surface and is 4 $cm^2$ in this case. Kline and McClintock Method [32] is applied to calculate the uncertainty.

$$\Delta q'' \Big/ q'' = \sqrt{\left(\frac{\Delta P_{out}}{P_{out}}\right)^2 + \left(\frac{\Delta A}{A}\right)^2} \tag{6}$$

$$(\Delta P_{out}) \Big/ P_{out} = \sqrt{\left(\frac{\Delta k_{Cu}}{k_{Cu}}\right)^2 + \left(\frac{\Delta T}{T}\right)^2 + \left(\frac{\Delta(\Delta x_{1s})}{\Delta x_{1s}}\right)^2} \tag{7}$$

$$\Delta h \Big/ h = \sqrt{(\Delta q/q)^2 + \left(\frac{\Delta(T_{sat})}{\Delta T_{sat}}\right)^2} \tag{8}$$

For all the measurements of HTC, heat flux and heat transfer rate, the confidence level was above 90%.

## 4. Results and discussion

To validate the experimental setup and procedure, the results of the P surface with widely accepted Rohsenow correlation [33], Fig. 2. Where q" represents the input heat flux and ΔT sat represents the wall superheat, that is the difference in temperature between the testing surface and saturation temperature of the working liquid. A well match performance can be seen for our testing setup with the standard Rohsenow correlation. The detail of the Rohsenow correlation and comparison procedure can also be found in previous literature of the same experimental setup [34,35].

In addition, prior to exploring the performance of GO nanofluid over M surface, it is essential to confirm the literature reported enhanced performance of M surface and GO nanofluid. Hence, NBHT for P, M and NP have been performed in this section before the detailed analysis of GO nanofluid over M surface.

### 4.1. Microporous surface and GO nanofluid performance

Deionized water has been used as a working fluid over the P and M surfaces. While for $N_P$, GO nanofluid was used as working fluid over P surface.

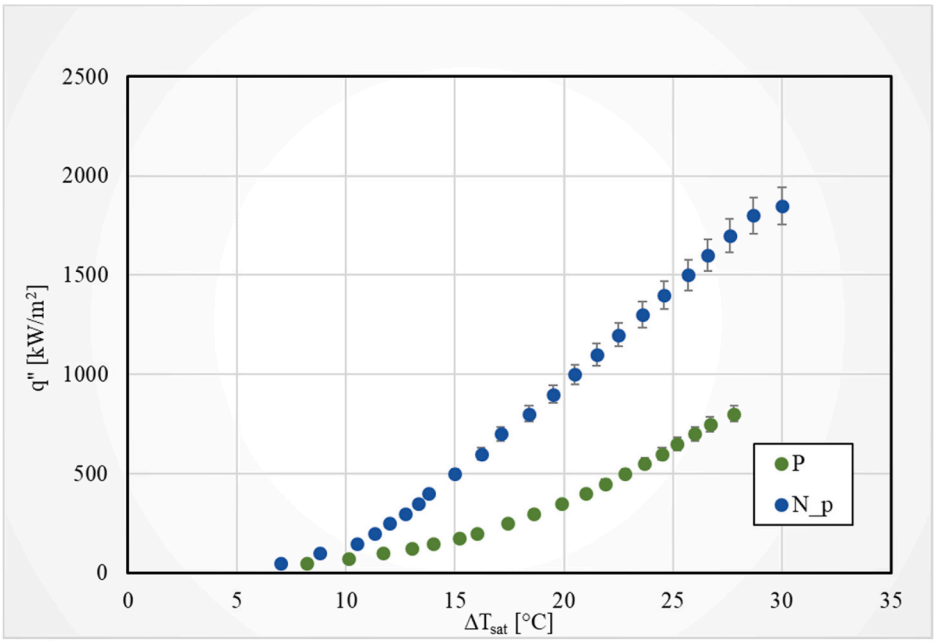


**Fig. 3.** Comparative analysis of nanofluid ($N_p$) and deionized water over plane (P) surface.

**GO nanofluid**: The performance of GO nanofluid in NBHT experiments can be analyzed in Fig. 3. Compared to the NBHT performance of P surface with deionized water, GO give rise to improved HTC and CHF. The CHF value for deionized water has been observed as 800 kW/m$^{2,}$ and for GO nanofluid, this value has been increased by *2.3* times to 1850 kW/m$^2$.

For GO nanofluid the enhanced performance is due to the deposition of GO nanofluid over P surface during NBHT experiments, Fig.3. The deposition of GO over P enhanced the overall surface area and acted as nucleation sites, raising bubbles concentration. Due to high departure frequency, it also results in the generation of the bubbles with a small diameter. The increase in bubble frequency represents the efficient heat removal from the heating surface, resulting in higher HTC. An increase in CHF can best represent the effect of delaying the film formation. The trend of increased performance is well matched with the literature reported enhanced GO nanofluid and M surfaces.

**Microporous surface**: The nucleate boiling heat transfer performance of the microporous surface (M) has been analyzed experimentally. The micro-porous surface resulted in superior CHF and average HTC. The average HTC for M porous surface has been increased by 3.47 times, Fig. 4. M surface's critical heat flux value has been increased by 1.40 times to 1120 kW/m$^2$, from 800 kW/m$^2$ of the plane surface. Due to the bubbles' early nucleation and efficient heat removal, the wall superheats value has been decreased by approximately 4.7 $^{o}$C at 100 kW/m$^2$.

The overall increase in performance of M surface is due to many factors including an overall increase in surface area, the microparticles act as nucleation points. In addition, the micro pores helps in providing discrete pathways for the flow of bubbles and liquid. It acts as an artery for the flow up going vapour and coming down the liquid. This results in efficient heat removal and postponements of film boiling hence improve HTC and CHF. There is also a slight decrease in the M surface's wettability to 120.2° form 100.9° of the P surface. However, the overall effect of M surface results in an enhancement of CHF value. Microparticles act as nucleation points hence increase the density of the bubbles. The formation of small bubbles results from the early departure of the bubbles and hence represents its higher frequency. This behavior of bubble dynamics symbolizes the efficient removal of the heat from the surface and hence higher HTC.

### *4.2. Hybrid (H) surface*

GO nanofluid over M surface in NBHT experiments resulted in the GO setting and led to the formation of the hybrid surface. Due to the high affinity of GO to the Cu the GO film and completely covered the top. The overall heat transfer ability of M surface has been affected severely, Fig. 5. The performance of the resulted surface has been declined by rise in the concentration of GO. For the highest concentration, of 0.01%, results in the lowest performance in HTC and the surface temperature has been crossed 50 °C of superheat value; hence the experiment has not proceeded to CHF. For the concentration of 0.01%, the average HTC value has decreased 0.17 times of M surface. For the concentration of 0.001%, the CHF value has been reduced to 426 kW/m$^2$ from 1120 kW/m$^2$, which is 0.38 times the M surface. For the concentration of 0.001%, the average HTC value has resulted in 0.17 times the M surface with deionized water.

The GO film formation, due to deposition on M surface, can be observed in Fig. 6. The micropores in M surface helps in the separation of bubbles and vapors and hence increase the CHF. Also, the role of microparticles for the nucleation of bubbles and

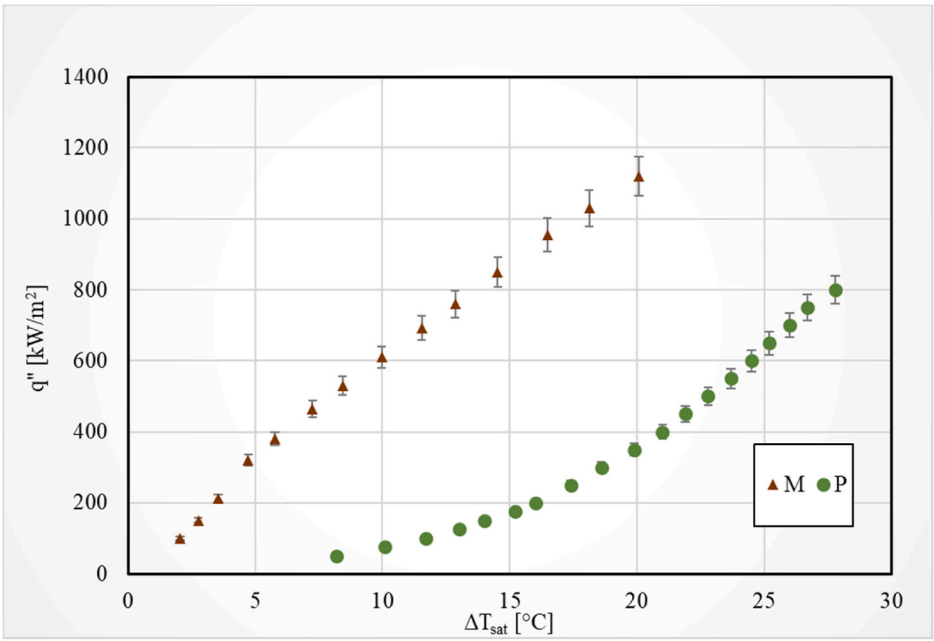


**Fig. 4.** Comparative analysis of microporous (M) and deionized water over plane (P) surface.

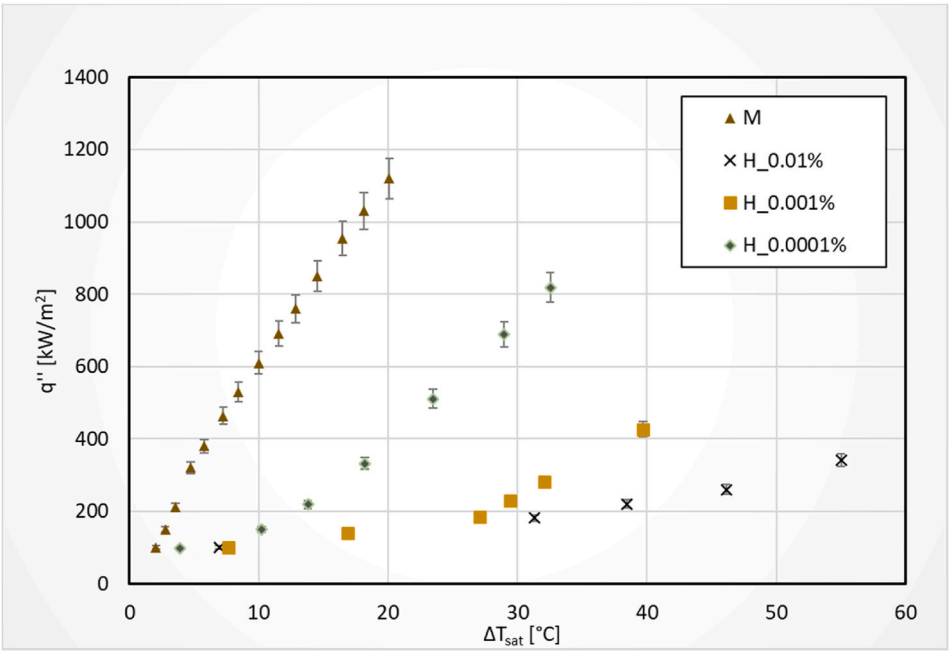


**Fig. 5.** NBHT curve for graphene oxide nanofluid as working fluid and microporous (M) surface.

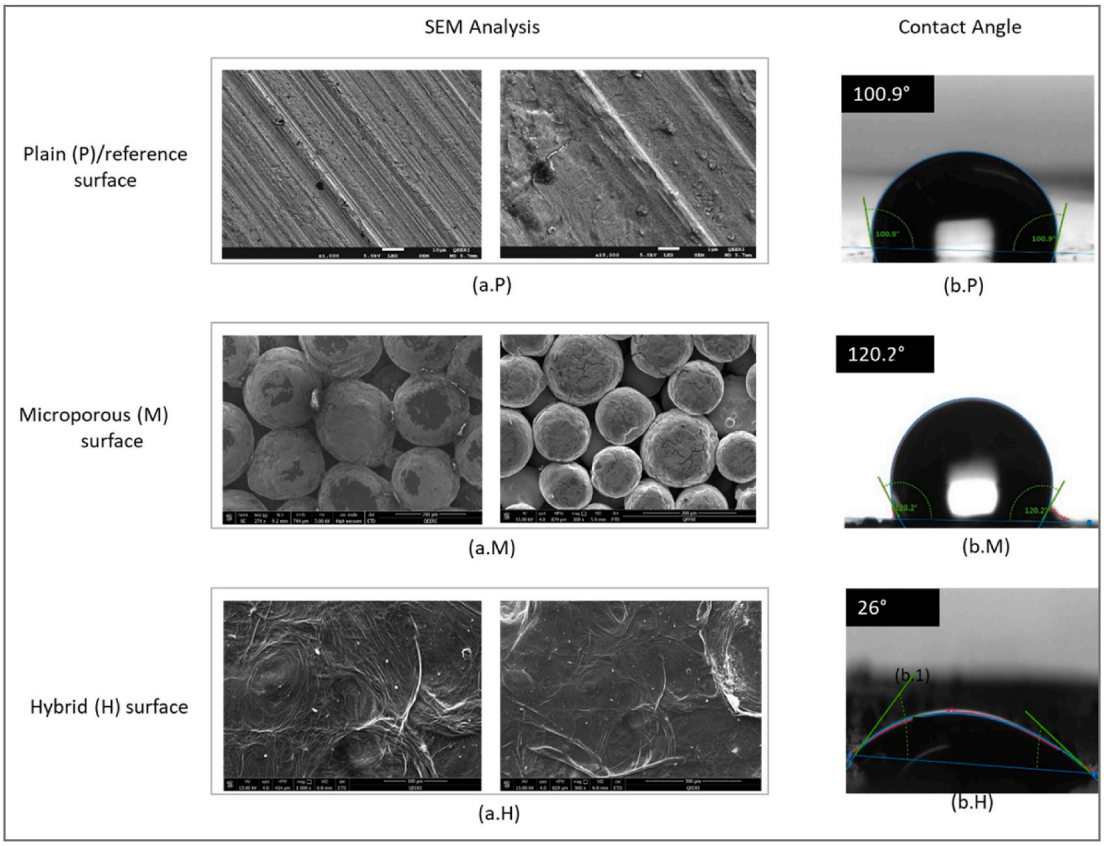


**Fig. 6.** Morphology of P, M and H surface and their corresponding contact angle.

generation of bubbles with small size and higher frequency results in efficient removal of heat and hence high HTC. However, GO deposition blocks the micropores and prevents the flow of bubbles and liquid, affecting the original designed phenomena of M surface. This prevented the proper formation of bubbles and their flow from the hot surface with increased input heat flux. Fig. 7 represents a clear difference in bubbles dynamics from M surface with deionized water and GO nanofluid. Fig. 7 illustrates the bubble's dynamics during NBHT at different heat fluxes, for the lowest concentration of 0.0001%, as for higher concentrations, the nanofluid was not transparent enough to observe. The lack of proper formation of the bubbles increased the surface temperature greater than the M surface with deionized water. This severely affected the efficiency of heat removal and hence average HTC value.

The overall performance and comparative analysis of all the four surface is represented in Table 2. Both M and $N_p$ resulted in an increase performance in CHF. The highest increase in HTC is of 64.36 [kW/m$^2$.K] is achieved by M surface with an increase of 3.47 times. While, the highest CHF value of 1850 [kW/m$^2$] is recorded for $N_p$ with a rise of 2.31 times. For GO, nanofluid over microporous surface resulted in decrease performance of HTC and CHF with a decrease of 0.17 and 0.38 times, respectively. The lowest average HTC value of 10.86 [kW/m$^2$.K] is noted for hybrid, GO nanofluid over M, surface.

## 5. Thermal management of CPV

The maximum ability of heat transfer and efficient heat removal are the key parameters of the thermal management system. In CPV system, both of these parameters are highly sensitive to the feasibility of CPV-based system installation. The maximum ability of heat transfer is directly related to the maximum possible concentration in CPV system. The increase in concentration decreases the required cell material in CPV system, which is the most expansive part in CPV. On the other hand, the efficient removal of heat flux results in lower cell temperature. Low cell temperature leads to higher efficiency and hence higher energy output.

NBHT based thermal management for CPV is considered with its effect installation area, efficiency and concentration ratio. The installation area and concentration ratio directly affect a photovoltaics-based energy system's economic and installation feasibility. The installation area is of specific importance for the installation in an area with limited availability. The maximum heat transfer ability of thermal management is directly related to the maximum concentration ratio in CPV. At the same time, the efficiency of the thermal management system is directly related to the CPV cell temperature and hence its electrical efficiency.

A CPV system with a multi-junction solar cell is considered, Table 3. The efficiency of cell directly depends upon the operating temperature of the cell and calculated by Ref. [36]:

$$\eta_{CPV} = \eta_{std,CPV} + \alpha(T_{cell} - T_{std}) \tag{9}$$

The maximum concentration ratio (C.R) for the CPV system is calculated by Ref. [37]:

$$C.R = \frac{q}{I_{DNI}\left(1 - \eta_{loss} - \eta_{std,CPV}\right)} \tag{10}$$

where q is CHF. The required area $A_{int}$ for the output power ($P_o$) is:

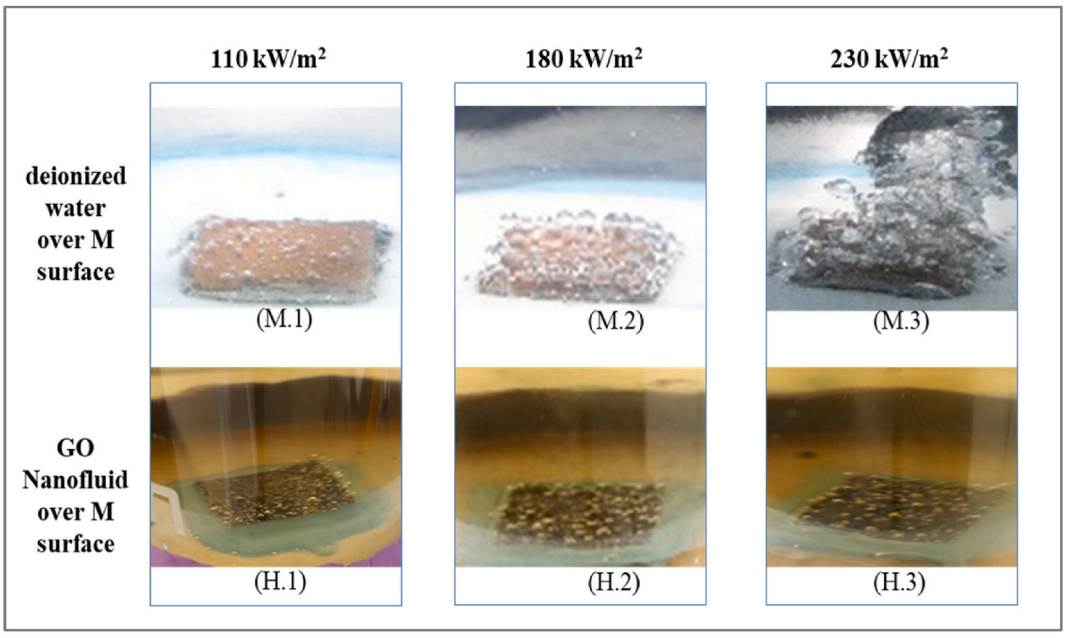


**Fig. 7.** Bubbles dynamics over microporous surface at three different input heat flux: (M.1), (M.2) and (M.3) represents deionized water as working; (H.1), (H.2), (H.3) are GO nanofluid as working fluid.

**Table 2**
CHF, HTC and their comparative analysis for all the tested surfaces.

| Surface | Plain (P) | Microporous (M) surface | GO Nanofluid (Np) surface | Hybrid: 0.001% GO nanofluid |
|---|---|---|---|---|
| CHF [kW/m$^2$] | 800.00 | 1120.00 | 1850.00 | 426.00 |
| $q_{CHF}/q_{CHF,P}$ | | 1.40 | 2.31 | 0.53 |
| $q_{CHF}/q_{CHF,M}$ | | | 1.65 | 0.38 |
| HTC average | 18.56 | 64.36 | 40.04 | 10.86 |
| Average (HTC/HTC$_P$) | | 3.47 | 2.16 | 0.58 |
| Average (HTC/HTC$_M$) | | | 0.62 | 0.17 |

**Table 3**
The considered CPV model in this study form [1].

| Parameter | Explanation/Value |
|---|---|
| Cell | NREL, inverted Metamorphic multijunction (IMM) solar cell |
| α: Thermal coefficient (%/K) | −0.052 |
| $\eta_{lstd.CPV}$: Standard electrical efficiency (%) | 40.8 |
| $T_{std}$: Standard testing temperature (°C) | 25 |
| $\eta_{loss}$: optical and thermal energy loss (%) | 10 |
| $I_{DNI}$: irradiation level (kW/m$^2$) | 1 |

$$P_o = \eta_{CPV} * I * A_{int} \tag{11}$$

The maximum concentration ratio is obtained by GO nanofluid ($N_p$) based thermal management system due to high CHF value. However, M resulted in higher efficiency than $N_p$ and P surface. The higher efficiency of M surface results from its higher HTC value and efficient removal of heat and lower cell temperature, Fig. 8. M surfaces increased the maximum concentration ratio of P surface from 1425 to 1894 with higher efficiency 0.6%. At the same time, $N_p$ resulted in the highest concentration ratio of 3102 with almost the same energy efficiency to P surface.

$N_p$-based thermal management is best feasible for the condition where a high concentration ratio is required to reduce the required cell material. This system can solve the feasibility of newly developed high-efficiency solar cells due to their high cost. Where M-based thermal management solution can be applied to the system with more significant high energy efficiency. The system can provide a solution to installing a CPV-based system where a lower installation area is more significant, i.e. urban infrastructure. Fig. 9 represents the comparative analysis of installation area for silicon-based solar cell, with maximum efficiency of 25%, and multijunction solar cell, Table 3, with M based thermal management system. The required installation area can be decreased by 63% by the use of multijunction based solar cell with the $N_P$ based nucleate boiling thermal management system. For example, for the installed area of 1000 m$^2$ the resulting electrical output for the M-based thermal management system of considered CPV is 41.2 MW while for silicon-based PV system is 25 MW.

## 6. Conclusion

Both microporous surfaces and GO-based nanofluid is well reported in the literature for enhanced NBHT performance. The study investigated the GO nanofluid performance in NBHT system over microporous surfaces. Three different nanofluid concentrations were tested in NBHT experiments over the microporous surface, along with the experiment analysis of GO nanofluid and M experimental performance. Experimental results are then a couple for thermal management of CPV using an analytical model of multijunction solar cell-based CPV system. The experimental results of the study are summarized below:

- Both M surface and GO nanofluid resulted over P surface resulted in an enhanced, as reported in the literature.
- However, the GO particles deposited on M surface and form a complete film of GO nanoparticles resulted in a hybrid (H) surface.
- The deposited GO nanoparticles severely affected the performance of M surface in terms of HTC and CHF. For the lowest nanofluid concentration with 0.01% the HTC value has been reported to be 0.38 times of M surface.
- For H surface, the increase in GO concentration resulted in a decrease in CHF and HTC.
- The maximum CHF value of 1850 kW/m$^2$ has been reported for GO over P surface with an enhancement of 2.31 times.
- The highest average HTC is reported for M surface with deionized water with an increase of 3.47 times.
- NBHT based thermal management system can play an essential role in the feasibility of CPV system's installation in urban infrastructure.
- $N_p$-based NBHT system can achieve a concentration ratio of more than 3000 and make economic feasibility for high efficiency multijunction solar cell in the CPV system.
- M-based NBHT thermal management system resulted in high efficiency in CPV system and can be used where installation area is limited.

NBHT system can play a significant role in the efficient removal and high heat flux removal from CPV. Both parameters play an

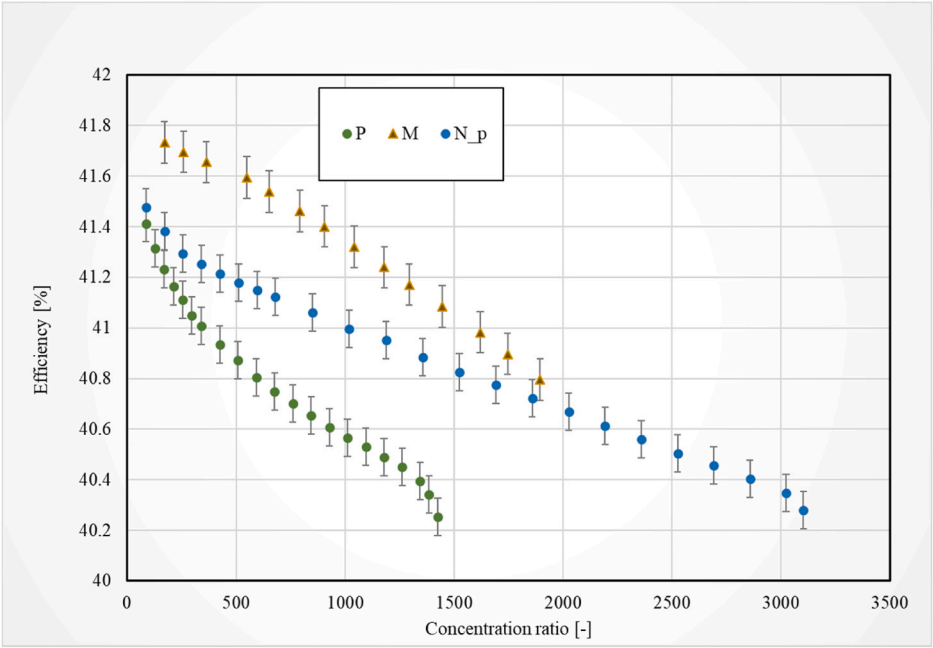


**Fig. 8.** Concentration ratio and respective efficiency of the considered CPV-based system with NBHT based thermal management system for P, $N_p$, and M surface.

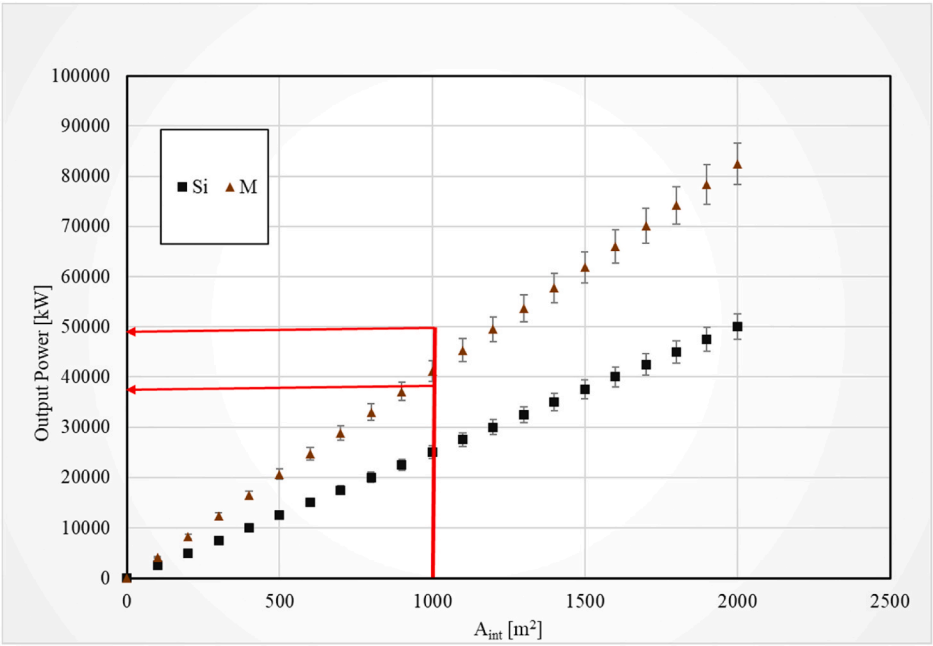


**Fig. 9.** The required installation area for electrical power output in considered multijunction solar cell based CPV system (M) and silicon solar cell based system. (For interpretation of the references to colour in this figure legend, the reader is referred to the Web version of this article.)

important role in the feasibility of a high-efficiency CPV system by reducing its cost and installation area. NBHT system with M surfaces resulted in higher efficiency among the compared solution. The maximum ability of concentration of 3102 is reported for $N_p$ surfaces. M based NBHT system can be applied for high efficiency where $N_p$ is best feasible for CPV system with high cost of solar cell. The M-based thermal management system can make the CPV-based renewable energy system feasible for the urban location where the available installation for renewable energy systems is a challenge.

**Future recommendation**. The direct coating of nanoparticles on microparticles could enhance surface area, roughness and

nucleation density. However, the challenge of microparticles coating without affecting the pores between the particles is still a challenge to be addressed. The coating of nanoparticles on the substrate before the synthesis of micro-porous surface can be a possible solution to attempt.

## Author statement

Shoukat Alim Khan: Methodology, Data curation, Investigation, Writing- Original draft preparation. Sami G. Al-Ghamdi: Conceptualization, Visualization, Supervision, Reviewing and Editing.

## Declaration of competing interest

The authors declare that they have no known competing financial interests or personal relationships that could have appeared to influence the work reported in this paper.

## Acknowledgment

The authors acknowledge the support of Hamad Bin Khalifa University, Qatar Foundation. The authors acknowledge the Qatar Environment and Energy Research Institute (QEERI) core lab for the SEM, performed by Mr. Mujaheed Pasha, and Mr. Muhammad I. Hilal and contact angle analysis by Dr. Ayman Samara. Open Access funding provided by Qatar National Library.

## Nomenclature

| | |
|---|---|
| Aint | Installation Area |
| CHF | Critical heat flux |
| CNT | Carbon nanotubes |
| CPV | Concentrated photovoltaics |
| DI | Deionized |
| GO | Graphene oxide |
| H | Hybrid |
| HTC | Heat transfer coefficient |
| KCu | Thermal conductivity |
| NBHT | Boiling Heat Transfer |
| Np | Nanofluid over plane surface |
| M | Microporous |
| MJSC | Multifunction solar cells |
| P | Plane unmodified |
| $T_{b.surface}$ | Temperature of the tasting sample |
| Tsat | Saturation temperature |
| $q''$ | Heat flux |
| ΔX12 | Distance between two thermocouples 1 and 2 |
| ΔX1s | Distance between thermocouple 1 and testing sample |
| η | Efficiency |

## References

[1] S.A. Khan, Y. Bicer, S.G. Al-Ghamdi, M. Koç, Performance evaluation of self-cooling concentrating photovoltaics systems using nucleate boiling heat transfer, Renew. Energy 160 (2020) 1081–1095, https://doi.org/10.1016/j.renene.2020.06.070.
[2] O. Rejeb, A. Radwan, E.M. Abo-Zahhad, C. Ghenai, A.A. Serageldin, M. Ahmed, et al., Numerical analysis of passive cooled ultra-high concentrator photovoltaic cell using optimal heat spreader design, Case Stud Therm Eng 22 (2020), 100757, https://doi.org/10.1016/j.csite.2020.100757.
[3] U. Sajjad, M. Amer, H.M. Ali, A. Dahiya, N. Abbas, Cost effective cooling of photovoltaic modules to improve efficiency, Case Stud Therm Eng 14 (2019), 100420, https://doi.org/10.1016/j.csite.2019.100420.
[4] I. Mudawar, Recent advances in high-flux, two-phase thermal management, J. Therm. Sci. Eng. Appl. 5 (2013), https://doi.org/10.1115/1.4023599.
[5] A. Riahi, A. Ben Haj Ali, A. Fadhel, A. Guizani, M. Balghouthi, Performance investigation of a concentrating photovoltaic thermal hybrid solar system combined with thermoelectric generators, Energy Convers. Manag. 205 (2020), 112377, https://doi.org/10.1016/j.enconman.2019.112377.
[6] F. Yazdanifard, M. Ameri, R.A. Taylor, Numerical modeling of a concentrated photovoltaic/thermal system which utilizes a PCM and nanofluid spectral splitting, Energy Convers. Manag. 215 (2020), 112927, https://doi.org/10.1016/j.enconman.2020.112927.
[7] M. Javidan, A.J. Moghadam, Experimental investigation on thermal management of a photovoltaic module using water-jet impingement cooling, Energy Convers. Manag. 228 (2021), 113686, https://doi.org/10.1016/j.enconman.2020.113686.
[8] S.A. Khan, M. Koç, S.G. Al-Ghamdi, Urban concentrated photovoltaics: advanced thermal management system using nanofluid and microporous surface, Energy Convers. Manag. 222 (2020), 113244, https://doi.org/10.1016/j.enconman.2020.113244.
[9] A. Kumar, A.K. Behura, D.K. Rajak, R. Kumar, M.H. Ahmadi, M. Sharifpur, et al., Performance of heat transfer mechanism in nucleate pool boiling -A relative approach of contribution to various heat transfer components, Case Stud Therm Eng (2020), 100827, https://doi.org/10.1016/j.csite.2020.100827.

[10] Y.-W. Lu, S.G. Kandlikar, Nanoscale surface modification techniques for pool boiling enhancement—a critical review and future directions, Heat Tran. Eng. 32 (2011) 827–842, https://doi.org/10.1080/01457632.2011.548267.
[11] G. Song, P.A. Davies, J. Wen, G. Xu, Y. Quan, Nucleate pool boiling heat transfer of SES36 fluid on nanoporous surfaces obtained by electrophoretic deposition of Al2O3, Appl. Therm. Eng. 141 (2018) 143–152, https://doi.org/10.1016/j.applthermaleng.2017.12.068.
[12] H.M. Ali, M.M. Generous, F. Ahmad, M. Irfan, Experimental investigation of nucleate pool boiling heat transfer enhancement of TiO 2 -water based nanofluids, Appl. Therm. Eng. 113 (2017) 1146–1151, https://doi.org/10.1016/j.applthermaleng.2016.11.127.
[13] S.K. Das, N. Putra, W. Roetzel, Pool boiling characteristics of nano-fluids, Int. J. Heat Mass Tran. 46 (2003) 851–862, https://doi.org/10.1016/S0017-9310(02)00348-4.
[14] S.M. You, J.H. Kim, K.H. Kim, Effect of nanoparticles on critical heat flux of water in pool boiling heat transfer, Appl. Phys. Lett. 83 (2003) 3374–3376, https://doi.org/10.1063/1.1619206.
[15] G. Liang, I. Mudawar, Review of pool boiling enhancement by surface modification, Int. J. Heat Mass Tran. 128 (2019) 892–933, https://doi.org/10.1016/j.ijheatmasstransfer.2018.09.026.
[16] J.H. Lee, T. Lee, Y.H. Jeong, The effect of pressure on the critical heat flux in water-based nanofluids containing Al2O3 and Fe3O4 nanoparticles, Int. J. Heat Mass Tran. 61 (2013) 432–438, https://doi.org/10.1016/j.ijheatmasstransfer.2013.02.018.
[17] Z.-H. Liu, X.-F. Yang, J.-G. Xiong, Boiling characteristics of carbon nanotube suspensions under sub-atmospheric pressures, Int. J. Therm. Sci. 49 (2010) 1156–1164, https://doi.org/10.1016/j.ijthermalsci.2010.01.023.
[18] R. Kamatchi, S. Venkatachalapathy, C. Nithya, Experimental investigation and mechanism of critical heat flux enhancement in pool boiling heat transfer with nanofluids, Heat Mass Tran. 52 (2016) 2357–2366, https://doi.org/10.1007/s00231-015-1749-2.
[19] S.D. Park, S.W. Lee, S. Kang, S.M. Kim, I.C. Bang, Pool boiling CHF enhancement by graphene-oxide nanofluid under nuclear coolant chemical environments, Nucl. Eng. Des. 252 (2012) 184–191, https://doi.org/10.1016/j.nucengdes.2012.07.016.
[20] N. Sezer, S.A. Khan, M. Koç, Amelioration of the pool boiling heat transfer performance by colloidal dispersions of carbon black, Int. J. Heat Mass Tran. 137 (2019), https://doi.org/10.1016/j.ijheatmasstransfer.2019.03.161.
[21] A. Rainho Neto, J.L.G. Oliveira, J.C. Passos, Heat transfer coefficient and critical heat flux during nucleate pool boiling of water in the presence of nanoparticles of alumina, maghemite and CNTs, Appl. Therm. Eng. 111 (2017) 1493–1506, https://doi.org/10.1016/j.applthermaleng.2016.06.130.
[22] S.A. Khan, N. Sezer, M. Koç, Design, fabrication and nucleate pool-boiling heat transfer performance of hybrid micro-nano scale 2-D modulated porous surfaces, Appl. Therm. Eng. 153 (2019), https://doi.org/10.1016/j.applthermaleng.2019.02.133.
[23] Pialago Ejt, O.K. Kwon, J.S. Jin, C.W. Park, Nucleate pool boiling of R134a on cold sprayed Cu-CNT-SiC and Cu-CNT-AlN composite coatings, Appl. Therm. Eng. 103 (2016) 684–694, https://doi.org/10.1016/j.applthermaleng.2016.04.022.
[24] R. Wen, Q. Li, W. Wang, B. Latour, C.H. Li, C. Li, et al., Enhanced bubble nucleation and liquid rewetting for highly efficient boiling heat transfer on two-level hierarchical surfaces with patterned copper nanowire arrays, Nanomater. Energy 38 (2017) 59–65, https://doi.org/10.1016/j.nanoen.2017.05.028.
[25] R. Wen, S. Xu, Y.-C. Lee, R. Yang, Capillary-driven liquid film boiling heat transfer on hybrid mesh wicking structures, Nanomater. Energy 51 (2018) 373–382, https://doi.org/10.1016/j.nanoen.2018.06.063.
[26] S.J. Thiagarajan, R. Yang, C. King, S. Narumanchi, Bubble dynamics and nucleate pool boiling heat transfer on microporous copper surfaces, Int. J. Heat Mass Tran. 89 (2015) 1297–1315, https://doi.org/10.1016/j.ijheatmasstransfer.2015.06.013.
[27] C.L. Tien, A hydrodynamic model for nucleate pool boiling, Int. J. Heat Mass Tran. 5 (1962) 533–540, https://doi.org/10.1016/0017-9310(62)90164-3.
[28] Ö.N.C. Koç, M. Yu and, Micro-manufacturing of micro-scale porous surface structures for enhanced heat transfer applications: an experimental process optimization study, J. Micromech. Microeng. 19 (2009) 45011, https://doi.org/10.1088/0960-1317/19/4/045011.
[29] Khan SA, Koc M. Synthesis and Testing of Graphene Hydrogel Surfaces for Nucleate Boiling Heat Transfer (NBHT) augmentation n.d.:120.
[30] S.A. Khan, N. Sezer, S. Ismail, M. Koç, Design , synthesis and nucleate boiling performance assessment of hybrid micro-nano porous surfaces for thermal management of concentrated photovoltaics (CPV), Energy Convers. Manag. 195 (2019) 1056–1066, https://doi.org/10.1016/j.enconman.2019.05.068.
[31] N. Sezer, S.A. Khan, M. Koç, Amelioration of the pool boiling heat transfer performance by colloidal dispersions of carbon black, Int. J. Heat Mass Tran. 137 (2019) 599–608, https://doi.org/10.1016/j.ijheatmasstransfer.2019.03.161.
[32] S.J. Kline Fam, Describing uncertainties in single-sample experiments, Mech. Eng. 75 (1953) 3–9.
[33] W.M. Rohsenow, A Method of Correlating Heat Transfer Data for Surface Boiling of Liquids, 1951. Cambridge.
[34] N. Sezer, S.A. Khan, M. Koç, Amelioration of the pool boiling heat transfer performance via self-assembling of 3D porous graphene/carbon nanotube hybrid film over the heating surface, Int. J. Heat Mass Tran. 145 (2019), https://doi.org/10.1016/j.ijheatmasstransfer.2019.118732.
[35] S.A. Khan, N. Sezer, M. Koç, Design, fabrication and nucleate pool-boiling heat transfer performance of hybrid micro-nano scale 2-D modulated porous surfaces, Appl. Therm. Eng. 153 (2019) 168–180, https://doi.org/10.1016/j.applthermaleng.2019.02.133.
[36] A. Royne, C.J. Dey, D.R. Mills, Cooling of photovoltaic cells under concentrated illumination: a critical review, Sol. Energy Mater. Sol. Cells 86 (2005) 451–483, https://doi.org/10.1016/j.solmat.2004.09.003.
[37] S.A. Khan, Y. Bicer, M. Koç, Design and analysis of a multigeneration system with concentrating photovoltaic thermal (CPV/T) and hydrogen storage, Int. J. Hydrogen Energy (2018), https://doi.org/10.1016/j.ijhydene.2018.12.047.